# The Source of the Midwinter Suppression in Storminess over the North Pacific

SANDRA PENNY

*Department of Atmospheric Sciences, University of Washington, Seattle, Washington*

GERARD H. ROE

*Department of Earth and Space Sciences, University of Washington, Seattle, Washington*

DAVID S. BATTISTI

*Department of Atmospheric Sciences, University of Washington, Seattle, Washington*

(Manuscript received 27 October 2008, in final form 3 August 2009)

ABSTRACT

Feature-tracking techniques are employed to investigate why there is a relative minimum in storminess during winter within the Pacific storm track (the midwinter suppression). It is found that the frequency and amplitude of disturbances entering the Pacific storm track from midlatitude Asia are substantially reduced during winter relative to fall and spring and that the magnitude of this reduction is more than sufficient to account for the midwinter supression. Growth rates of individual disturbances are calculated and compared to expectations from linear theory for several regions of interest. Although there are discrepancies between linear expectations and observed growth rates over the Pacific, the growth of disturbances within the Pacific storm track cannot explain why the midwinter suppression exists. Furthermore, it is determined that the development of a wintertime reduction in storminess over midlatitude Asia is consistent with linear expectations, which predict a wintertime minimum in Eady growth rates in this region, mainly because of increased static stability. Several other mechanisms that may contribute to the initiation of the midwinter suppression over midlatitude Asia are discussed, including the interaction between upper-level waves and topography, the behavior of waves upwind of the Tibetan Plateau, and the initiation of lee cyclones.

## 1. Introduction

The midwinter suppression of the Pacific storm track[1] is a striking phenomenon for which a complete explanation has proven elusive. In the midlatitudes, temperature gradients and jet stream winds reach a maximum in the middle of winter. A simple interpretation of the linear Eady model of baroclinic storm formation and growth (Eady 1949; Lindzen and Farrell 1980) predicts that midlatitude storminess should also maximize at this time and it does throughout much of the Northern Hemisphere. In the western Pacific, however, many standard Eulerian measures of storminess (e.g., variance of geopotential height) exhibit a relative minimum in winter compared with fall and spring (Fig. 1a).

Nakamura (1992) first identified the midwinter suppression and, since then, substantial progress has been made in characterizing it. It has been observed that, when the strength of the wintertime jet stream exceeds $\sim$45 m s$^{-1}$, the correlation between the zonal wind at 250 hPa and many common measures of storminess becomes negative (Nakamura 1992). In addition, a similar relationship exists for interannual variability: years with a strong midwinter suppression tend to exhibit stronger than normal jet stream winds (e.g., Chang 2001; Nakamura et al. 2002). Christoph et al. (1997) found that the suppression is not a statistical artifact by noting that it exists in frequencies well outside the range of a typical bandpass filter. Furthermore, the midwinter suppression

[1] There is some ambiguity in the meaning of the phrase storm track. In this study, we reserve "storm track" to refer to the geographic region of enhanced synoptic activity in the climatological sense (as is conventional in climate literature) and not the path of an individual storm. Related to this, we refer to the amount of synoptic activity in a storm track as the amplitude of "storminess."

*Corresponding author address:* Sandra Penny, Dept. of Atmospheric Sciences, University of Washington, 408 ATG Bldg., Box 351640, Seattle, WA 98195-1640.
E-mail: smpenny@atmos.washington.edu

DOI: 10.1175/2009JCLI2904.1

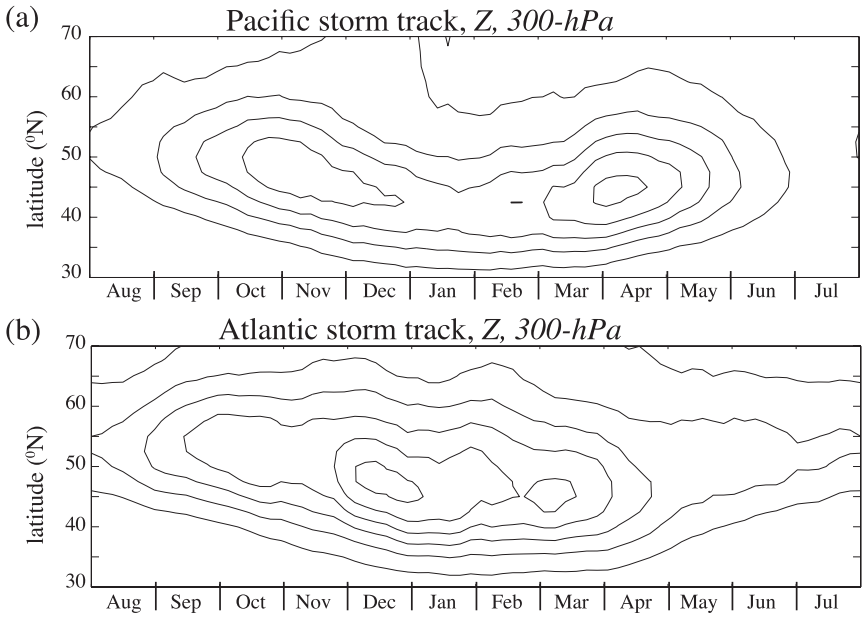


FIG. 1. Midwinter suppression of the Pacific storm track, shown as the variance in geopotential height at 300 hPa: (a) Pacific domain (20°–70°N, 140°E–180°) and (b) Atlantic domain (20°–70°N, 30°–70°W). The contour interval is 1500 $m^2$ starting at 2000 $m^2$. This is an update of Fig. 2 in Nakamura (1992) for the ERA-40 dataset between 1958 and 2001. The data are 2–6 day bandpass filtered using a fourth-order Butterworth filter to obtain daily climatologies. Results are smoothed with a 31-day running mean filter and plotted every five days. Large tick marks on the abscissa correspond to the first day of each month.

is a robust feature of the atmospheric circulation that is observed in both reanalysis data and in output from general circulation models (e.g., Nakamura 1992; Zhang and Held 1999; Chang 2001; Yin 2002).

Numerous publications have evaluated how the midwinter suppression may arise through various dynamical mechanisms that occur within the Pacific storm track. A large body of work evaluates the possibility that the faster, narrower, more subtropical wintertime jet stream causes the midwinter suppression. The strong wintertime jet stream, which results in 15% faster group velocity of wave packets within the storm track (Chang 2001), causes propagating waves to be advected quickly through regions of strong baroclinicity and may result in reduced spatial growth rates. However, Nakamura et al. (2002) considered both the increase in group velocity and the increase in expected Eady growth rates and found that the two together can only explain 5% of the interannual variability between strong and weak January storm activity. Harnik and Chang (2004) explored whether modifications to the linear models accounting for a narrower, faster jet stream could explain the midwinter suppression. They concluded that this may be important for interannual variability but the width of the jet stream does not vary enough from fall to spring for it to be of central importance. Deng and Mak (2005) studied a linear $\beta$-plane model and found that deformation associated with the strong, narrow wintertime jet stream could be an important factor in the midwinter supression. However, other analyses showed that this process may actually work in the wrong direction for the seasonal cycle of the Pacific storm track (Chang 2001; Yin 2002; Chang and Zurita-Gotor 2007)—transient waves in the Pacific storm track should lose less energy to the background flow in winter than in fall or spring. Finally, Nakamura and Sampe (2002) showed that the equatorward displacement of the wintertime jet stream causes disturbances to become trapped within a strong subtropical waveguide during winter. They point out that the more subtropical nature of the wintertime jet stream may be important to understanding the midwinter suppression.

Several studies have evaluated the role of diabatic effects in modulating the seasonal cycle of storm activity over the Pacific Ocean. Results drawn from a variety of analysis methods, a broad range of data sources, and a comprehensive hierarchy of models show that dry dynamics alone cannot fully explain the seasonal cycle of midlatitude storm activity (Zhang and Held 1999; Chang 2001; Yin 2002; Chang and Song 2006; Chang and Zurita-Gotor 2007). However, the extent to which moist dynamics is responsible for the midwinter suppression is still a subject of debate.

Finally, several studies have shown that seed disturbances are an important control on the strength of a storm track (e.g., Orlanski 2005; Zurita-Gotor and Chang 2005), and it has been suggested that the midwinter suppression could be the consequence of wave activity upwind of the Pacific storm track. Several studies have noted that a wintertime minimum in Eulerian variance extends well into Asia (e.g., Nakamura 1992; Zhang and Held 1999; Orlanski 2005); however, attempts to directly connect seeding with the midwinter suppression have not been conclusive. Zurita-Gotor and Chang (2005) showed that the coexistence of small eddy variance with large baroclinicity may be expected in the presence of local damping, such as observed over the Asian continent in winter. Robinson and Black (2006) found evidence that the central magnitude of cyclonic perturbations entering the Pacific storm track during winter is reduced relative to fall and spring. In addition, Robinson et al. (2006) demonstrated that specific patterns in the wintertime mean circulation over Siberia, perhaps associated with modulations of the East Asian winter monsoon, can precede intense wave activity downwind in the Pacific storm track. In a study focusing on the synoptic development of individual troughs, B. Myoung and J. W. Nielsen-Gammon (2009, personal communication) found that deformation may play a role in suppressing the intensity of disturbances upwind of the Pacific storm track.

The work mentioned above makes a significant contribution to our current understanding of the dynamics that control midlatitude storminess. However, when taken together, the literature gives the impression that there is no dominant underlying source of the midwinter suppression but that it is the result of several processes that combine to produce a wintertime minimum in synoptic-scale variance.

We demonstrate in this study that a clear picture of the midwinter suppression emerges when feature tracking is employed to characterize the western Pacific storm track. We find no evidence that the structure or growth rate of individual features within the Pacific storm track gives rise to the midwinter suppression. Rather, we show that the predominant source of the midwinter suppression of storminess in the western North Pacific is a reduction in the number and amplitude of seed disturbances that enter the Pacific during winter compared to fall and spring. Further analyses demonstrate that this is likely due to the seasonality in the interaction between surface static stability, the orography, and upper-level waves over Asia.

## 2. Methods

Storm tracks are usually defined as bands of higher than normal synoptic-scale baroclinic wave activity. In the climate literature they are predominantly characterized by Eulerian eddy statistics, usually calculated as the variance in a field (such as sea level pressure or heat transport) that has been bandpass filtered to isolate wave activity on the time scale of synoptic storms (e.g., Blackmon 1976; Blackmon et al. 1977). However, with the recent introduction of accurate feature-tracking algorithms, it is now possible to objectively calculate storm tracks from the individual disturbances that constitute them.

We have used the feature-tracking algorithm written by Kevin Hodges (Hodges 1994, 1995, 1999) to compile an inventory of all Northern Hemisphere disturbances in the 6-hourly 40-yr European Centre for Medium-Range Weather Forecasts (ECMWF) Re-Analysis (ERA-40) dataset (Uppala et al. 2005) from 1958 to 2001. The algorithm is well documented in the above references, so we give only a brief description here.[2] After removing a background state, the tracking algorithm first identifies all extrema above and below a user-specified threshold value in each time frame for the chosen field. Individual feature paths are then compiled using two constraints—smoothness of track and appropriate velocity—which are chosen adaptively for each disturbance. Finally, all disturbances that do not travel at least 1000 km and last 2 days are rejected.

In seeking to track synoptic-scale features, it is necessary to subtract a background state; this is done by preprocessing the data with a temporal or spatial filter. For geopotential height, we subtract the seasonal cycle by applying a 90-day highpass butterworth filter to the data, then we apply a spatial filter that admits only planetary wavenumbers between 5 and 42. Our choice here is somewhat unusual, so a brief discussion is warranted.

For our purposes, a standard temporal filter such as a 2.5–6-day bandpass filter (e.g., Blackmon 1976; Blackmon et al. 1977) is not ideal because it overemphasizes the wavelike nature of the atmosphere and artificially adds disturbances where none existed in the original field. This is only a small disadvantage for Eulerian calculations, where storminess is measured by the standard deviation of a field, but this is an undesirable effect when tracking features. To avoid such complications, Hoskins and Hodges (2002, 2005) and Anderson et al. (2003) advocate the use of a spatial filter that admits planetary wavenumbers between 5 and 42. However, Donohoe and Battisti (2009) recently showed that this spatial filter leaves time-average features in the core of

[2] The seasonal climatologies of feature-tracking results from the ERA-40 dataset are available for download from K. Hodges, Web site.

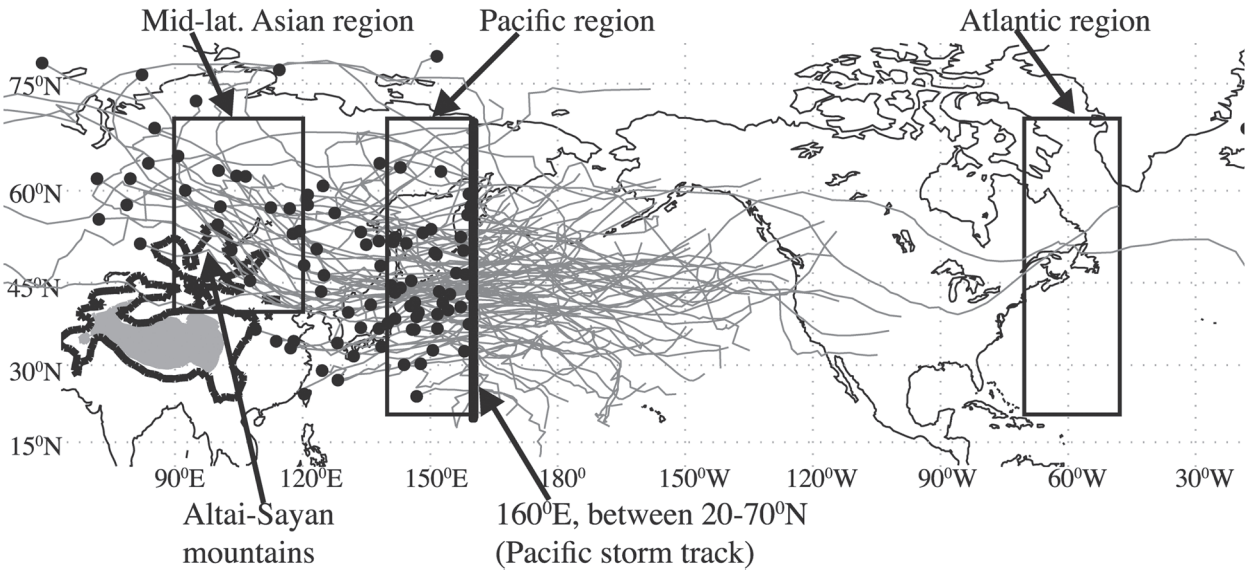


FIG. 2. Sample of the individual disturbances (randomly selected from the month of November) that cross 160°E between 20° and 70°N (thick black line). Black dots denote the genesis location and the gray line indicates the path of an individual disturbance. The contour is for 1.5-km topography; shading indicates topography higher than 3 km. Boxed regions correspond to the areas where statistics are compiled for the Pacific, Atlantic, and midlatitude Asian regions in Fig. 7.

the Pacific and Atlantic storm tracks [$O$(10 hPa) or more for the field of sea level pressure], which significantly affects the number and magnitude of the identified features.

We have avoided these difficulties by combining both spatial and temporal filtering. Application of a 90-day highpass filter decreases the amplitude of time-averaged spatial features by almost two orders of magnitude, from around 10 to 0.3 hPa, without affecting synoptic motions (not shown). This weak temporal filtering effectively eliminates the largest drawback associated with a planetary spatial filter, while retaining its advantages over a 2.5–6-day bandpass filter.

In the results section below, we primarily analyze tracking results derived from upper-level (300 hPa) geopotential height cyclonic disturbances. Results from relative vorticity are also discussed in appendix A. Synoptic disturbances in these two fields are ideal to track because features have an easily identified center and central magnitude is a meaningful measure of intensity. The minimum threshold value (relative to the background field) for the existence of a feature is chosen as 3 dm for geopotential height and $10^{-5}$ s$^{-1}$ for relative vorticity. We find that the algorithm is insensitive to any reasonable choice of threshold and that the lifetime and track length requirements ensure that only substantial disturbances are included in the analysis.

We define the western Pacific storm track as being comprised of disturbances that cross longitude 160°E between 20° and 70°N. This choice is made to focus on the region that has strong midwinter suppression in the eddy statistics (see Fig. 1). For illustration, Fig. 2 shows a sample of the paths of cyclonic disturbances (randomly selected from the month of November) tracked in geopotential height at 300 hPa. The analysis is not sensitive to this choice of longitude. Similar results are obtained when performing the same analysis throughout the western and central Pacific.

Results are also insensitive to the latitudinal range, for example, results are essentially the same if tracking all disturbances between 20° and 70°N, or only those located within 10° to the north and south of the climatological storm track axis. Results found using the whole record (1958–2001) also hold for the satellite era (1979–2001). Though most of the results presented here are found in the field of geopotential height, we have performed similar calculations using relative vorticity and meridional and zonal wind at levels between 250 and 500 hPa. Tracking results from these fields (not shown) are very similar. Some interesting considerations for tracking relative vorticity are included in appendix A.

## 3. The midwinter suppression characterized by the number and amplitude of disturbances

The midwinter suppression of the Pacific storm track was first identified by Nakamura (1992), and his calculation is reproduced in Fig. 1 (updated to include data from the ERA-40 dataset, 1958–2001). Over the North Atlantic Ocean, upper-level geopotential height variance

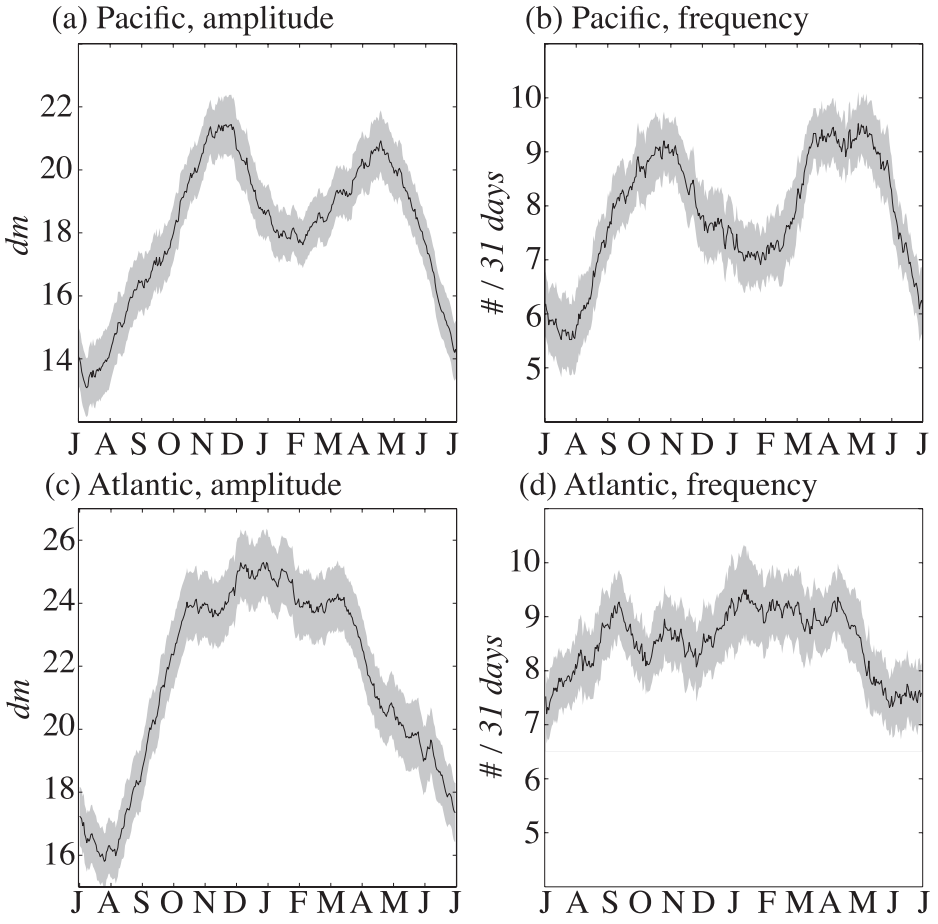


FIG. 3. Seasonal cycle of the features identified in the geopotential height field at 300 hPa: (a) mean amplitude [this is the magnitude (dm) at the center of the disturbance] as disturbances cross 160°E (Pacific storm track), (b) mean monthly frequency as disturbances cross 160°E, (c) mean amplitude (dm) as disturbances cross 50°W (Atlantic storm track), and (d) mean monthly frequency as disturbances cross 50°W. Daily climatologies are smoothed with a 31-day running mean smoother. Tick marks correspond to the first day of each month; shading indicates 95% confidence intervals as calculated from the Student's *t* test.

is maximized in the middle of winter, whereas over the western North Pacific it peaks during fall and spring. Along longitude 160°E between 20° and 70°N (marked as the bold line in Fig. 2), the variance of geopotential height at 300 hPa is reduced by approximately 25% in winter relative to the shoulder seasons (see appendix B for details about this calculation).

Feature tracking enables changes in storminess to be studied in detail. In particular, it is possible to isolate the relative importance of changes in feature frequency and changes in feature strength, which is impossible using Eulerian eddy statistics alone. In appendix B, we discuss the connection between Eulerian variance and the results obtained by feature tracking.

We obtain climatological data on the frequency of occurrence and the average central magnitude of all disturbances that cross 160°E and 50°W for the Pacific and Atlantic storm tracks for each calendar day: these results are shown in Fig. 3. A 31-day running mean smoother is applied before plotting the results to reduce noise and to represent the data as monthly averages. Over the Atlantic Ocean feature strength is maximized during winter, and feature number exhibits little seasonality. In contrast, the disturbances within the Pacific storm track show a clear reduction in both number (~20%) and amplitude (~14%) during winter compared to spring and fall. These results are robust well above the 95% confidence level determined from a Student's *t* test (shading in Fig. 3) and are observed in all locations throughout the western North Pacific domain from 120°E to 160°W (not shown).

Nakamura (1992) speculated that a wintertime lull in the generation of seed disturbances over Asia could play

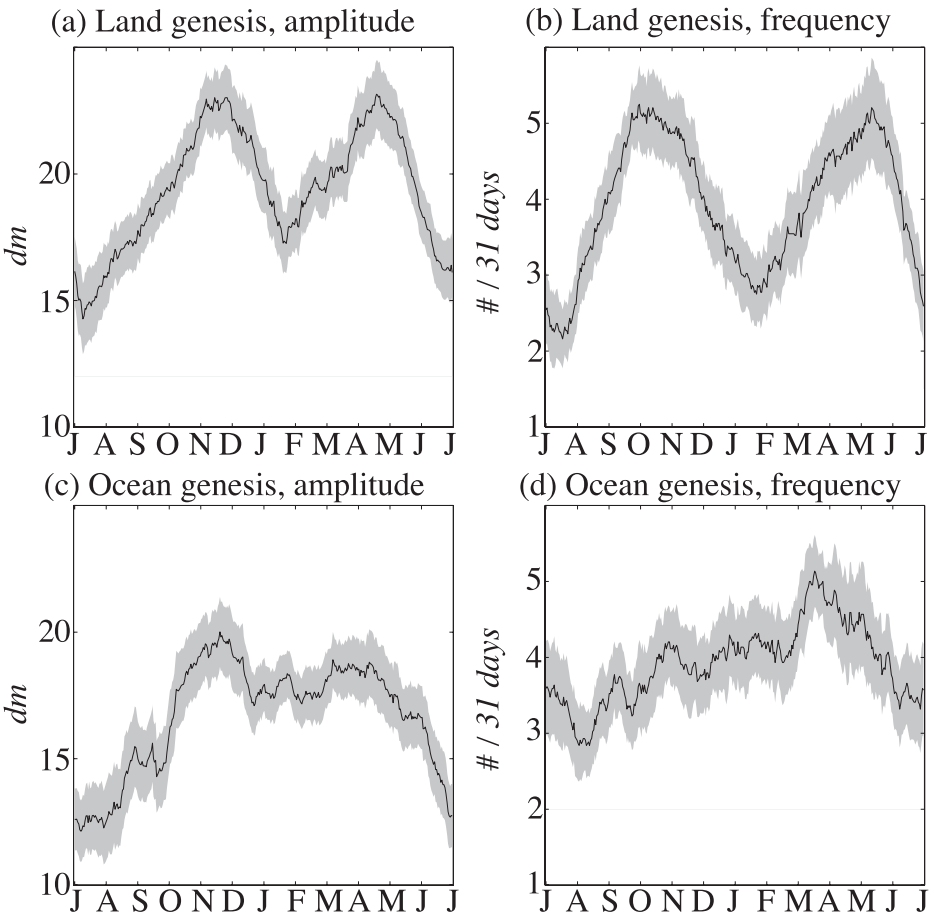


FIG. 4. As in Fig. 3 but for Pacific storm track features that (a),(b) originated over land and (c),(d) originated over the ocean.

a role in the suppression of storminess in the western Pacific. We investigate this possibility by separating the Pacific disturbances that originate over land from those that originate over water, shown in Fig. 4. The frequency of cyclogenesis[3] over the Pacific steadily increases from October ($\sim$3 month$^{-1}$) through April ($\sim$5 month$^{-1}$), and the amplitude of these disturbances exhibits a small, but not statistically significant, minimum during the winter months. On the other hand, cyclogenesis frequency over land is significantly reduced in midwinter relative to fall and spring, by about 40% in frequency and 20% in amplitude. This is a strong indication that a reduction in the frequency of seed disturbances from Asia is responsible for the midwinter suppression.

The presence of the Tibetan Plateau causes the storm track over Asia to split into two branches: a midlatitude branch to the north and a subtropical branch to the south. It is widely accepted that the storm track over the Pacific Ocean is primarily seeded by waves propagating from the midlatitude branch over northeast Asia (e.g., Wallace et al. 1988; Hakim 2003; Chang 2005), but recent work shows that wave activity within the Pacific storm track can be seeded by both branches (Hoskins and Hodges 2002; Chang 2005). We also find that disturbances that exist over the western and central Pacific Ocean can have both midlatitude and subtropical origins. We investigate the relative importance of the northern and the southern branch (Fig. 5) and then consider the impact of influences upwind of Tibet (Fig. 6).

The features that cross 160°E between 20° and 70°N are separated by their latitude of cyclogenesis, using 40°N as the dividing line, in Fig. 5. Consistent with previous studies, the midlatitude branch comprises the majority of the disturbances downwind in the Pacific storm track. Both frequency and amplitude of disturbances that originate to the north of 40°N show a clear wintertime reduction. In contrast, the number of features that originate south of 40°N steadily increases from

[3] We define cyclogenesis location as the location that the tracking algorithm first identifies a feature.

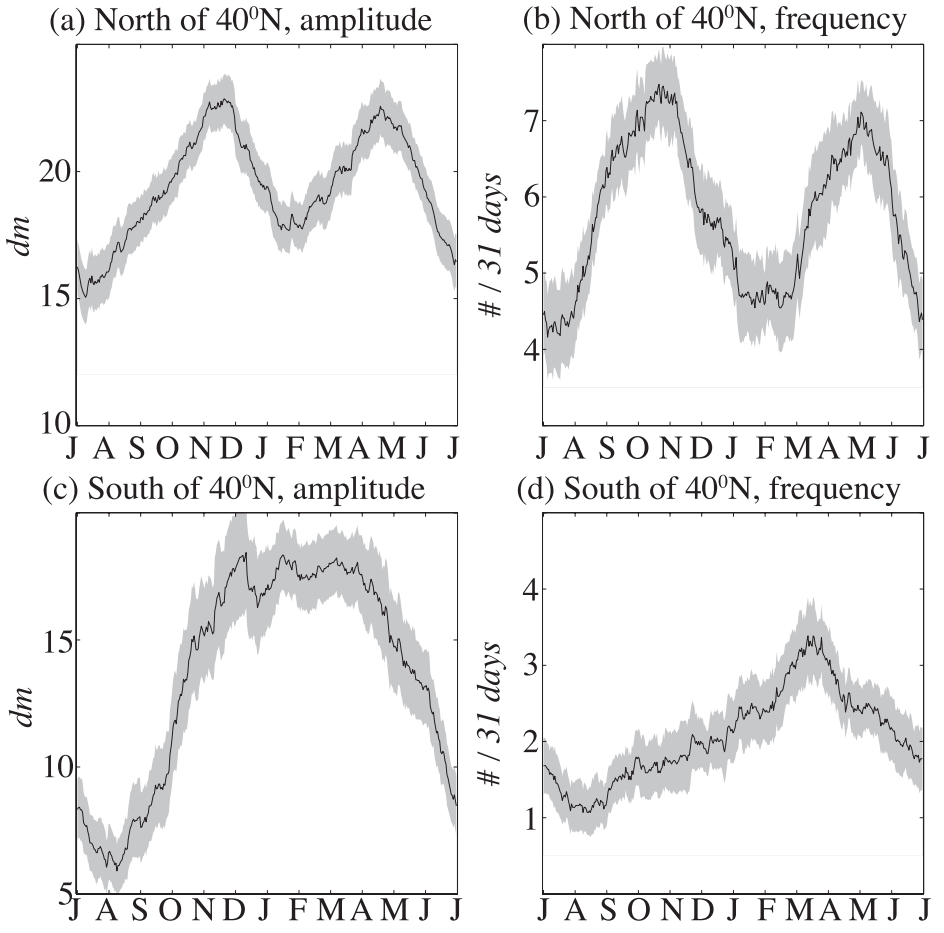


FIG. 5. As in Fig. 3 but for Pacific storm-track features that had their genesis (a),(b) north of 40°N and (c),(d) south of 40°N.

fall to spring and the amplitude of these features is largest during the winter months. This strongly suggests that the midwinter suppression is not caused by changes in subtropical cyclogenesis and/or subtropical seeding.

Next, we calculate the frequency and amplitude of features upwind of the Tibetan Plateau, as they cross 60°E (Figs. 6a,b), and downwind, as they cross 120°E (Figs. 6c,d). Upwind of the plateau there is a maximum in the number of disturbances during winter and a maximum in their amplitude during fall. This is in contrast to the situation directly downwind of the Tibetan Plateau where the midwinter suppression is clearly seen as the midwinter reduction of both the frequency and amplitude. Certainly, some aspects of the seasonality in storminess are difficult to understand with simple theory (e.g., we have not explained why the number of subtropical disturbances maximizes in spring). However, the above discussion and results show that the midwinter suppression in storminess over the North Pacific Ocean has its origins over midlatitude Asia, to the north of the Tibetan Plateau.

## 4. The role of changes in growth rates for the midwinter suppression

We have shown that the midwinter suppression can be understood by considering the behavior of upper-level waves upwind of the Pacific storm track. Therefore, there is no need to invoke changes in the development of disturbances within the storm track itself as an explanation. Nonetheless, several studies have found compelling evidence that the seasonal cycle of the background flow may modify the structure and growth rate of baroclinic waves within the Pacific storm track in a way that causes the midwinter suppression (e.g., Nakamura 1992; Christoph et al. 1997; Chang 2001; Yin 2002).

To investigate this with our dataset, we calculate the growth rates of the tracked features and compare them to the theoretical Eady growth rates in Fig. 7. All calculations in Fig. 7 are performed within a ''Pacific region'' (20°–70°N, 140°–180°E), an ''Atlantic region'' (20°–70°N, 30°–70°W), and a ''midlatitude Asian region'' (40°–70°N,

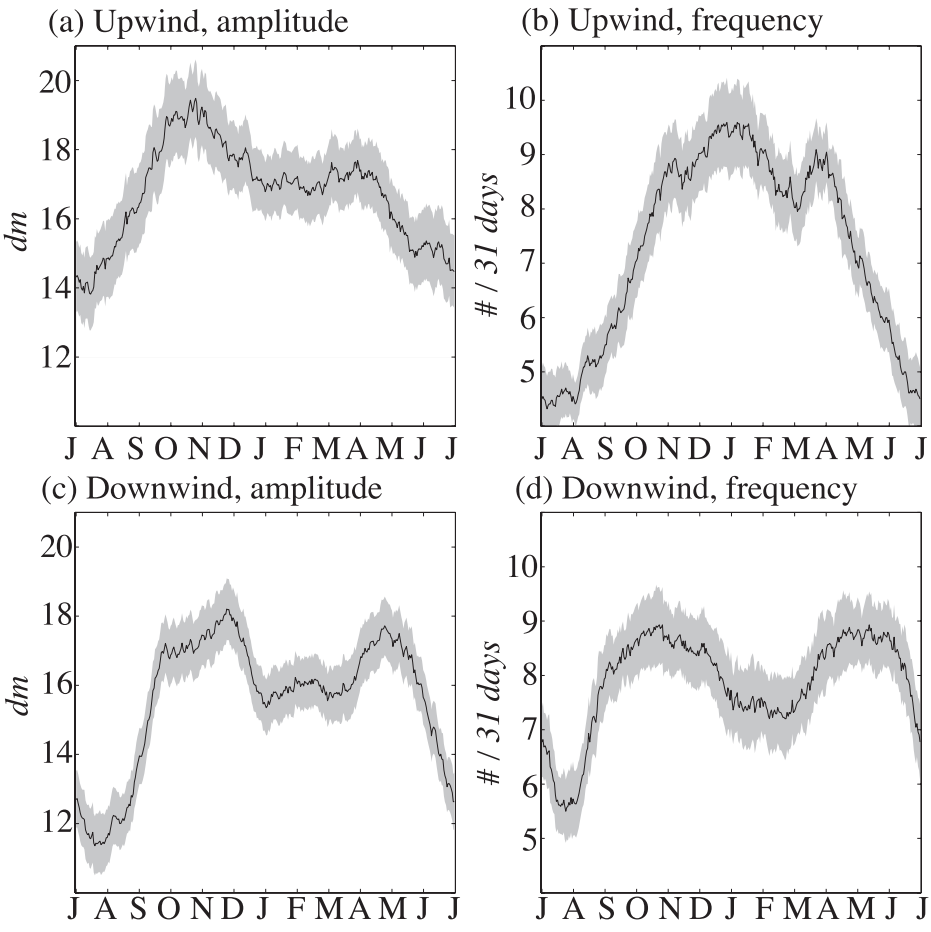


FIG. 6. As in Fig. 3 but for Pacific storm-track features (a),(b) upwind (as they cross 60°E) of the Tibetan Plateau and (c),(d) downwind (as they cross 120°E) of the Tibetan Plateau.

90°–120°E)–these regions are indicated by boxes in Fig. 2.

We measure the growth rate of the tracked features of each growing upper-level cyclonic feature in Bergerons [Bergeron = $(\Delta Z/6\text{ h})\sin 60°/\sin(0.5\Delta\Phi)$], which is equivalent to the change in central amplitude ($\Delta Z$) over each 6-h period normalized by a factor proportional to the change in the Coriolis parameter ($\Phi$ is latitude). Note that the observed growth rate is independent of changes in the speed of disturbances; that is, the fact that features are traveling faster over the oceans during winter than they are in the shoulder seasons (e.g., Chang 2001) does not affect this calculation.

Growth rates predicted from the theoretical Eady model (referred to as the ''traditional Eady growth rate'') are expressed as a fractional growth rate, following the methods outlined in Lindzen and Farrell (1980):

$$\sigma_{\mathrm{MAX}} = 0.31\frac{f}{N}\frac{\partial \overline{u}}{\partial z}, \qquad (1)$$

whereas the observed growth rate of tracked features is an absolute growth rate. To express these two measures with the same units (dm $h^{-1}$), we define an ''adjusted Eady growth rate'' as the product of the traditional Eady growth rate and the average disturbance amplitude from the feature-tracking algorithm. The observed and adjusted Eady growth rates are co-plotted in Figs. 7a,d,g. For reference, the traditional Eady growth rate (Figs. 7c,f,i) and the monthly averaged feature amplitude of growing disturbances (Figs. 7b,e,h) are also shown.

The adjusted and traditional Eady growth rates are computed for a near-surface layer. This layer lies between 925 and 850 hPa for the Pacific and Atlantic regions and between 850 and 700 hPa for the midlatitude Asian region. A near-surface layer is chosen because Nakamura and Shimpo (2004) found that near-surface Eady growth rates are well correlated with jet-stream-level wave activity.

Within the Atlantic region (Fig. 7d) there is a wintertime maximum in the growth rate of individual disturbances

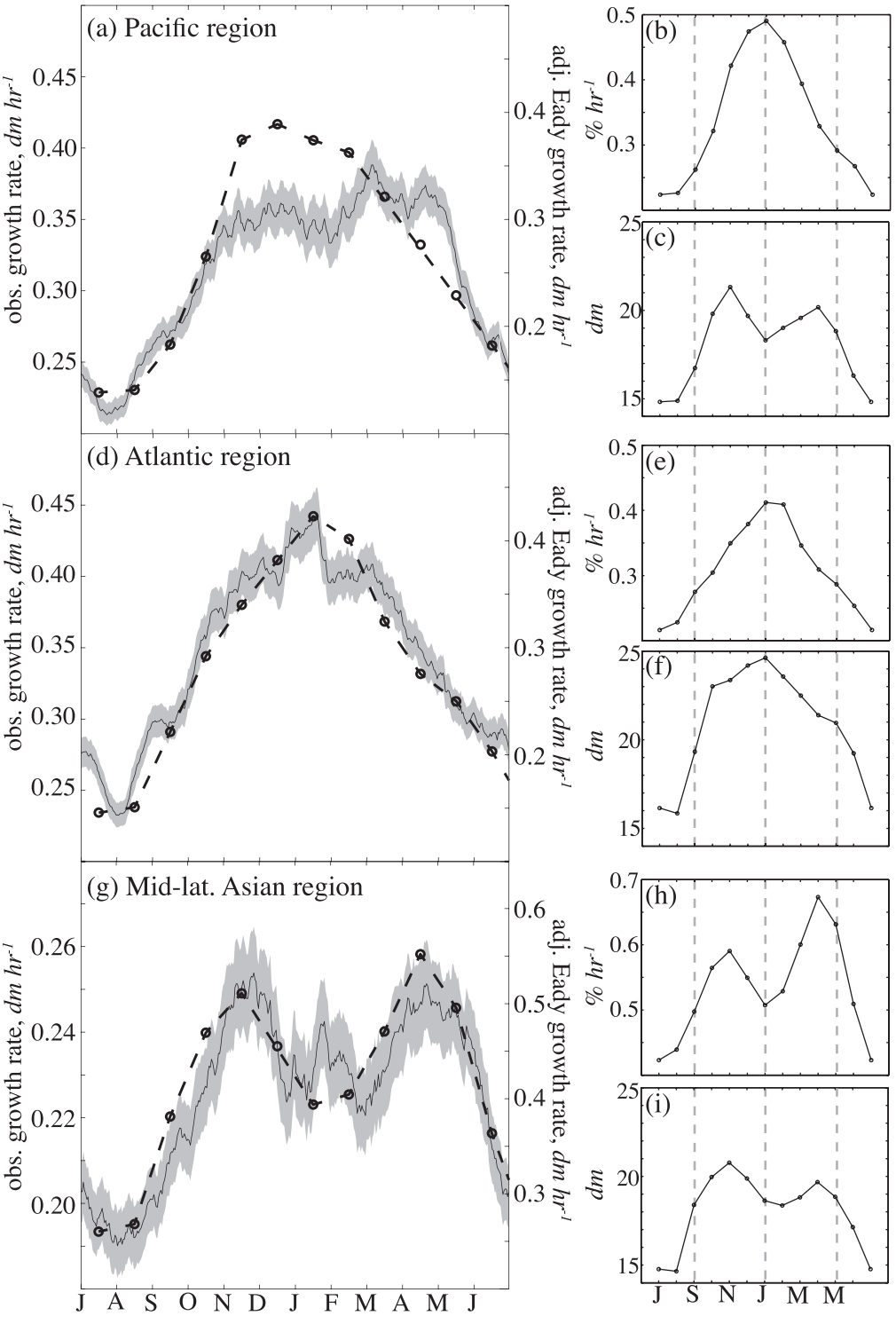


FIG. 7. Comparison between the observed growth rate in $Z$ at 300 hPa (dashed lines) and the near-surface adjusted Eady growth rate (solid line with gray shading for 95% confidence) scaled to fit on the same figure for (a) the Pacific region (20°–70°N, 120°–160°E), (d) the Atlantic region (20°–70°N, 70°–30°W), and (g) the midlatitude Asian region (40°–70°N, 90°–120°E). The monthly average near-surface traditional Eady growth rates are shown for the (b) Pacific, (e) Atlantic, and (h) midlatitude Asian regions. The monthly average feature amplitude of growing disturbances in $Z$ at 300 hPa are shown for (c) the Pacific, (f) the Atlantic, and (i) the midlatitude Asian regions. Eady growth rates are calculated for the layer (a)–(e) between 925 and 850 hPa and (g)–(h) between 850 and 700 hPa.

and this corresponds well with expectations from linear theory. The same is not true over the Pacific Ocean; while the adjusted Eady growth rate maximizes during winter, observed growth rates are relatively constant through the cold season except for a marked springtime maximum (Fig. 7a). A springtime maximum in observed growth rates is also evident when we consider only the top 1% or 10% of growth rates, and it is robust to the choice of location and calculation method (e.g., for growth rates averaged over hours 6–48 of the storm's lifetime, including or excluding negative growth rates, choice of vertical levels, etc.). Furthermore, disturbances in the Atlantic region exhibit much larger amplitudes than those in the Pacific, even though Eady growth rates are largest in the Pacific region. Thus, the results do show that there is a discrepancy between observed growth rates and linear expectations. However, the absence of a midwinter minimum in the average growth rate of growing upper-level disturbances over the western and central Pacific (Fig. 7a) means the midwinter suppression cannot be due to reduced growth rates within the Pacific storm track.

For the midlatitude Asian region there is a marked and statistically significant suppression in both actual and expected Eady growth rates (Fig. 7g). Therefore, our finding that the midwinter suppression in the amplitude of disturbances in the Pacific storm track develops over midlatitude Asia (Figs. 3a, 4a, 5a, and 6c) is consistent with linear expectations. For example, consider the idealized case of disturbances traveling approximately 12 m $s^{-1}$ along 50°N between 90° and 120°E (a distance of approximately 3700 km, which is about half of the distance that a disturbance in this region typically travels in its lifetime). For features initially at 90°E with identical amplitudes, the observed reduction in wintertime growth rates of 0.03 dm $h^{-1}$ (Fig. 7g) would result in a 2.5-dm reduction in amplitude of the disturbances arriving at 120°E. This compares very well with the actual reduction in amplitude during winter, shown in Fig. 6c. Note that this argument only relates to why a midwinter suppression in feature amplitude develops over midlatitude Asia. Most individual disturbances do not travel from across Asia all the way to the Pacific storm track. However, we observe a very similar seasonal cycle in growth rates if we limit our analysis in Fig. 7g to only include features that also make it into the Pacific storm track.

The adjusted and traditional Eady growth rates are presented only for diagnostic purposes, and there are several reasons for this. The Eady model assumptions are only strictly valid for small disturbances in their initial linear phase of growth, whereas we have included all growing disturbances in our calculation. Furthermore, although our results show that the Eady model is a good diagnostic tool for estimating the seasonality of monthly averaged growth rates, it is not a good indicator of growth rates for individual events. Within the Pacific and Atlantic regions, for example, the correlation between the observed growth rate and the Eady model prediction at the same time and location is found to be between only 0.15 and 0.20 (not shown). For this calculation, we have included only small (<5 or 10 dm) growing disturbances, and the actual correlation varies depending on the region and vertical level. Although small, this correlation is statistically significant at well above 99% confidence owing to the large number of disturbances included in the analysis.

## 5. Mechanisms that could explain the midwinter suppression

The last two sections identified the source of the midwinter suppression: a wintertime minimum in the number of disturbances born in northern Asia and tracking into the Pacific together with a wintertime minimum in the growth rate of these disturbances. We now discuss some mechanisms that could cause this reduction in the genesis and growth rate of these storms.

The wintertime minimum in Eady growth rates over midlatitude Asia (Fig. 7h) suggests that conditions are less favorable for cyclogenesis, which helps explain the midwinter suppression in the number of disturbances in this region. The quantitative contributions to the Eady growth rate [Eq. (1)] from both shear and stability are determined by the relationship

$$\frac{\Delta\sigma}{\overline{\sigma}} \approx \frac{\Delta\lambda}{\overline{\lambda}} - \frac{\Delta N}{\overline{N}}, \tag{2}$$

where $\lambda = \partial\overline{u}/\partial z$, $\Delta$ notation corresponds to departures from the annual mean, and the overbar denotes the annual mean (Fig. 8). Surprisingly, shear maximizes in November; nonetheless, the wintertime minimum in Eady growth rates is dominated by the seasonality of near-surface static stability. Consistent with this finding, Nakamura et al. (2002) demonstrated that interannual variability associated with the midwinter suppression is anticorrelated with the strength of a stationary feature: the East Asian winter monsoon. In their paper, they identify East Asian winter monsoonal flow as strongly influenced by the Siberian high pressure system, which is a near-surface layer of stable air that is ultimately maintained by continental heating and cooling. These observations all support the possibility that seasonal modulations in static stability and patterns of high pressure over Asia play a central role in causing the midwinter suppression.

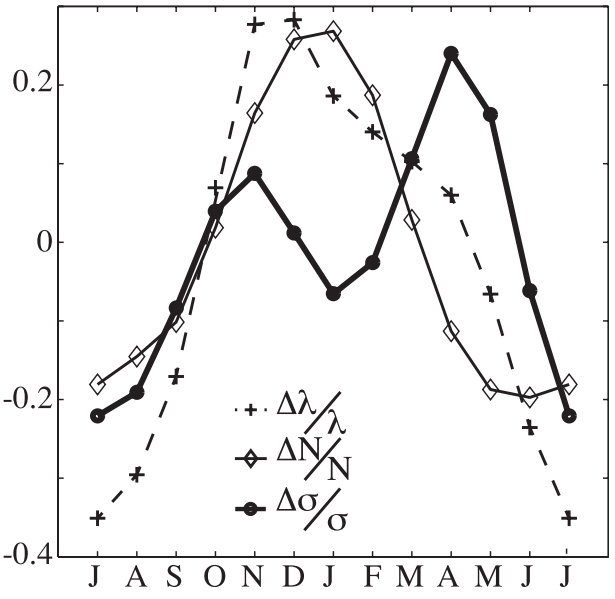


FIG. 8. Seasonal cycle of near-surface traditional Eady growth rates (circles) for the midlatitude Asian region (40°–70°N, 90°–120°E), as calculated by Eq. (2), along with contributions from the Brunt–Väisälä frequency (diamond) and shear (dashed-plus). The calculations are for the layer between 850 and 700 hPa, and the units correspond to the fractional departure of each variable from its annual mean.

A second possible mechanism, also directly related to near-surface effects, concerns the seasonal cycle in lower-tropospheric cyclogenesis in the lee of the Altai-Sayan mountains (identified in Fig. 2). Hoskins and Hodges (2002) used feature tracking to show that the genesis of midlatitude lower-tropospheric cyclones is concentrated in the lee of mountains. Chen et al. (1991) showed that there are significantly fewer Altai-Sayan lee cyclones in winter than fall or spring, and Newton (2004) noted that there is a striking correlation between the midwinter suppression over the Pacific Ocean and the generation of Altai-Sayan lee cyclones. Related to this, Roe (2009) argued that lee cyclogenesis in this region may be suppressed during winter because most of the continent is cold and strong temperature gradients lie well to the south (contributing to the wintertime minimum in Eady growth rates). By contrast, strong surface temperature gradients are frequently observed during fall and spring.

To establish the connection between Altai-Sayan lee cyclones and the upper-level waves that make up the midwinter suppression, we have performed composite analyses of the upper-level circulation at the time of lower-level lee cyclogenesis. These results (not shown) demonstrate that lee cyclogenesis is usually accompanied by a significant (~7 hPa) upper-level low oriented 200–300 km to the west of its low-level counterpart, an indication that upper and lower levels are in a position to mutually reinforce each other. Taken together, these results strongly suggest that lee cyclones play an active role in the development of the midwinter suppression.

Finally, influences upwind of the Tibetan Plateau may also contribute to the winter minimum in the number of disturbances. Hakim (2003) found that a large fraction of wave packets upwind of the Tibetan Plateau are diffracted into the subtropical jet stream and decay before entering the Pacific storm track. We have investigated whether waves are preferentially diffracted into the strong subtropical jet core over central Asia in winter. Preliminary results (not shown) show that this may also play a role in the development of the midwinter suppression.

## 6. Summary

The midwinter suppression in storminess over the western and central Pacific Ocean is due to a reduction in the number and amplitude of disturbances entering the Pacific storm track from midlatitude Asia. Feature tracking reveals that the number and amplitude of disturbances within the Pacific storm track in winter are reduced by 15%–43% and 12%–24% compared to the shoulder seasons, respectively. The exact percentage depends on the variable, level, and geographic location analyzed. The reduction in the number and amplitude of disturbances within the Pacific storm track is sufficient to explain the observed midwinter reduction in eddy variances documented here and previously (see appendix B for a comparison between feature tracking and Eulerian variance).

The midwinter reduction in the number and amplitude of storms within the Pacific storm track is not due to local changes in the synoptic-scale dynamics associated with seasonal changes in the structure of the jet: for example, there is no midwinter minimum in the growth rate of synoptic disturbances within the storm track (Fig. 7a). Instead, the reduction in the amplitude of features in the Pacific storm track is due to a midwinter minimum in the growth rate of the features that emanate from midlatitude Asia (Fig. 7g).

The winterime maximum in continental static stability is strongly implicated as the predominant cause of the midwinter suppression. The impact may manifest directly through reduced growth rates or indirectly through the interaction of surface stability, orography, and upper-level waves. The relative importance of these mechanisms remains to be explored.

There are many ways of characterizing storminess in the atmosphere and the correct choice is not always obvious. The use of Eulerian statistics has predominated in the study of climatological storminess, in part because

of its ease of calculation from reanalysis datasets and in part because such statistics are required in calculating heat and momentum budgets of the atmospheric circulation. However, Eulerian eddy statistics conflate many different aspects of the synoptic systems of which that climatology is comprised. These aspects may be of separate interest. For example, storm number, storm intensity, storm speed, and storm extent are all folded into the Eulerian statistics. In many regards, feature tracking provides a more fundamental perspective on storminess because it can more directly target the aspects of dynamical weather systems that are felt most keenly by observers on the ground—in other words, the high precipitation, high winds, strong frontal passages, etc., during individual storms. The availability of high-quality feature-tracking algorithms, therefore, provides many new and interesting opportunities for future research.

*Acknowledgments.* The authors are very grateful to Kevin Hodges for allowing us to use his feature-tracking algorithm, for his assistance with the program's use, and for helpful comments on an earlier version of this paper. Aaron Donohoe contributed to many discussions about this work. This draft was significantly improved by helpful comments and suggestions from Greg Hakim, Edmund Chang, Justin Minder, John Nielsen-Gammon, and an anonymous reviewer. This work was funded by the National Science Foundation Continental Dynamics Grant 6312293.

## APPENDIX A

### Tracking Results for Upper-Level Relative Vorticity

Parallel results concerning the reduction in the number and amplitude of disturbances during winter in the Pacific are found when tracking upper-level cyclonic relative vorticity[4] disturbances instead of geopotential height features. It is again clear that the midwinter suppression is primarily a consequence of there being fewer and smaller disturbances in winter than in fall and spring (Figs. A1a,b) and that the reductions are due to effects over land (not shown for relative vorticity). However, there are some important and interesting differences in the tracking results for geopotential (Fig. 3) and relative vorticity (Fig. A1) at the same pressure level (300 hPa). First, the tracking algorithm identifies almost twice as many disturbances in relative vorticity. This is not surprising since vorticity features are smaller in spatial scale than geopotential height features.

Second, it is perhaps surprising that the amplitude of relative vorticity features is actually an absolute minimum during winter, relative even to summer (Fig. A1a). This is not an artifact of the feature-tracking algorithm: the variance of 2–6-day bandpass filtered relative vorticity at 300 hPa is also an absolute minimum in winter at this location (not shown). We should be cautious about the interpretation of any measure of storminess if it indicates that the Pacific storm track is more intense during summer than it is in the middle of winter.

Scaling arguments having to do with the seasonal cycle of an average feature's areal extent can explain these peculiar results. In the geostrophic limit, relative vorticity is the Laplacian of geopotential height divided by the Coriolis parameter and this scales as geopotential height divided by a characteristic spatial scale:

$$\xi_{\text{geo}} = \frac{\nabla^2 \Phi}{f} \sim \frac{\Phi}{\text{area} \times f}. \tag{A1}$$

Consequently, for two features with the same central magnitude in geopotential height, the one that occupies less area actually has a larger central magnitude in relative vorticity. To determine the importance of the seasonal cycle of the average area of disturbances, we use tracking results to identify the center of all features as they cross various longitude bands within the Pacific storm track (i.e., 160°E, 180°) and employ compositing to estimate their average area (not shown). This reveals that the areal extent of disturbances during summer is just over half that of winter. In addition, in October and April features occupy approximately 14% less area than they do in January (not shown), so we cannot ignore this effect for the midwinter suppression. Evidently, we should be cautious in the interpretation of the variance of relative vorticity as a measure of storminess when the areal extent of waves changes significantly.

A notable seasonal cycle to the area of synoptic waves in the atmosphere was discussed to some extent by Hoskins and Hodges (2005), but to our knowledge this has never been examined in detail. Further, both meridional and zonal extent of disturbances is maximal in winter, which is surprising because the jet stream is narrower in winter than it is in the shoulder seasons.

[4] For tracking features in relative vorticity we take a rather minimalist approach to filtering. The data are first truncated to T42 resolution to reduce noise, and then we subtract out the seasonally varying background field by applying a 90-day highpass Butterworth filter. Others have found that filtering the field of vorticity can be unnecessary for some applications (e.g., Hakim 2003); however, without a seasonal mean filter, significant amplitude time-average features (of the order $\sim 2 \times 10^{-5}$ s$^{-1}$) are retained in the heart of the Pacific storm track, and this is something that we wish to avoid for feature tracking.

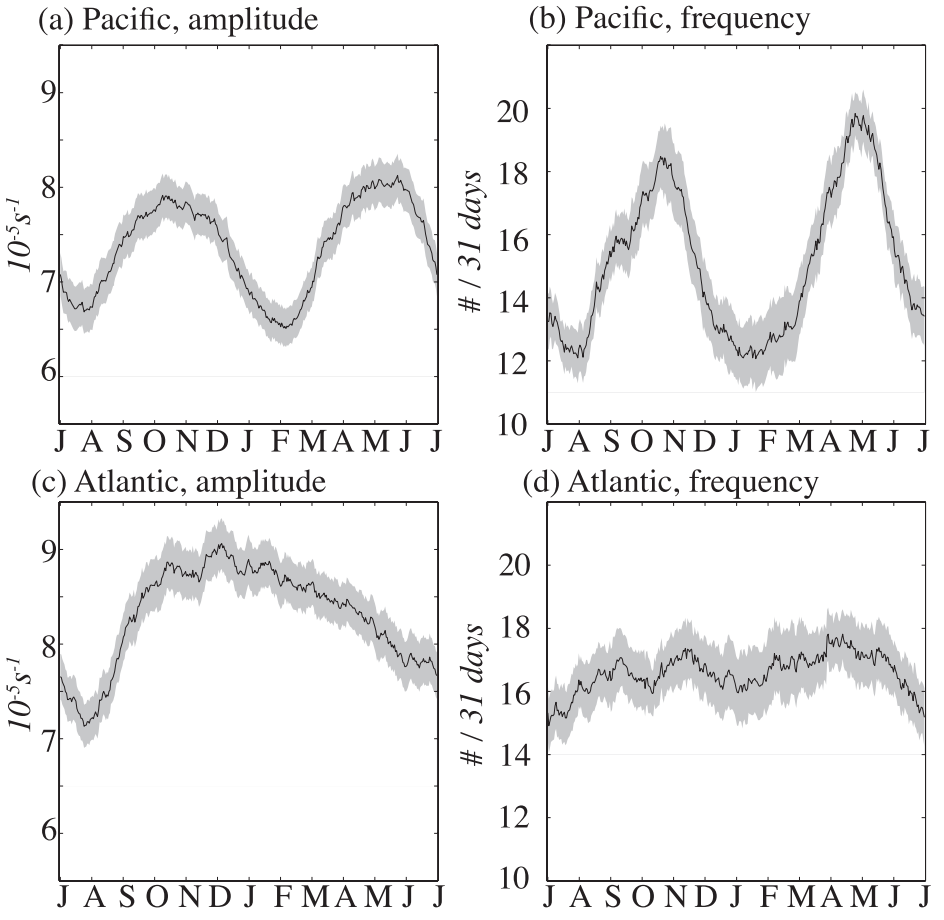


FIG. A1. As in Fig. 3 but for relative vorticity at 300 hPa. Units in (a) and (c) are $10^{-5}$ $s^{-1}$.

Ioannou and Lindzen (1986) found that the meridional extent of the jet stream is a reasonable first-order approximation to the meridional wavelength of storms. Based on these results, previous work concerning the midwinter suppression assumed that the meridional wavelength of storms in the Pacific storm track will be less in winter than it is in the shoulder seasons (Harnik and Chang 2004), an assumption that does not appear to be true in this region.

## APPENDIX B

### Comparing Eulerian Variance with Feature-Tracking Statistics

Our intention has been to understand how the midwinter suppression manifests in the individual disturbances that make up the Pacific storm track. However, it is also worth considering how the results from feature tracking compare with Eulerian variance at the same location.

To make a rough comparison we use the simple analogy of a traveling wave. Consider a single sine-shaped pulse with period $\tau$ traveling by a point (take $x = 0$ for simplicity) in the time interval $[0, T]$, where $\tau \ll T$:

$$Z = Z_0 \sin\frac{2\pi ct}{\lambda}, \quad 0 < t < \tau. \tag{B1}$$

The variance at this location owing to a single traveling pulse is

$$\overline{(Z')^2} = Z_0^2 \overline{\sin^2\frac{2\pi ct}{\lambda}}, \tag{B2}$$

where $c$ and $\lambda$ are the velocity and wavelength of the traveling wave, respectively, $Z_0$ is its amplitude, and $\overline{()} = T^{-1}\int_T () \, dt$ is the integral over the time of interest, $T$. In this framework, if the number of traveling sine-shaped pulses ($N$) doubles, then there is twice as much variance. Therefore, the total variance must scale linearly with the number of disturbances passing overhead. Noting that $\int_T \sin^2(at) \, dt = 1/(2a)$, we see that Eulerian variance is proportional to feature tracking in the following way:

TABLE B1. A comparison between feature-tracking statistics and Eulerian variance at 160°E between 20° and 70°N. Relative change is the average value during winter (Julian days 10–35) divided by the average value during fall and spring (days 300–325 and 90–115); $B_{\mathrm{LAGR}}$, defined by Eq. (B4) and explained in the text, is the relative change in Eulerian variance that is predicted by the feature-tracking statistics, and $\overline{(Z')^2}$ is the observed relative change in Eulerian variance at the same location.

| | Magnitude ($Z$) | Number ($N$) | Wavelength ($\lambda$) | Velocity ($c$) | $B_{\mathrm{LAGR}}$ | $\overline{(Z')^2}$ |
|---|---|---|---|---|---|---|
| Relative change | 0.86 | 0.80 | 1.07 | 1.03 | 0.61 | 0.75 |

$$\overline{(Z')^2} \propto NZ_0^2\lambda c^{-1}. \tag{B3}$$

We now compare storminess in winter to the average during fall and spring by defining

$$B_{\mathrm{LAGR}} \equiv \frac{\overline{(Z'_{\mathrm{wint}})^2}}{(Z'_{\mathrm{fall+spr}})^2}. \tag{B4}$$

Eulerian variance is compared to feature-tracking results in Table B1. For these calculations, variance of geopotential height at 300 hPa is the average in the 2–6-day bandpass filtered field along 160°E between 20° and 70°N. Data for the number, magnitude, wavelength, and velocity are average values for all disturbances as they cross the same location, 160°E between 20° and 70°N. Wavelength is interpreted as the characteristic length scale and approximated as the square root of the area of the disturbance, and area is estimated as outlined in appendix A. In Table B1, fall corresponds roughly to the month of November (Julian days 300–325), winter corresponds to January (days 10–35), and spring corresponds to April (days 90–115). From this information, we see that feature-tracking statistics predict that the midwinter suppression should manifest as a 39% reduction in the Eulerian variance in winter relative to fall and spring. In other words, this is 14% higher than the observed 25% reduction in wintertime variance.

There are several reasons not to expect these calculations to be directly comparable. First, in this paper the focus is on cyclonic disturbances only; yet, variance is a combination of both cyclones and anticyclones. Analysis of the number and amplitude of anticyclones at this location (not shown) reveals that high pressure systems do not exhibit a midwinter suppression. Second, Lagrangian statistics include only trackable, mobile disturbances, whereas there is no such requirement for Eulerian techniques. Third, for feature tracking we have employed both a seasonal-mean filter and a planetary wave filter (see discussion in the methods section); however, Eulerian variance is traditionally measured as the variance of a bandpass-filtered field (for our variance calculations we use a 2–6-day bandpass filter). Finally, and perhaps most importantly, we have greatly simplified the relationship between Eulerian variance and feature tracking by assuming that storm tracks are composed entirely of a series of identical nonoverlapping sine-shaped pulses. In reality, the amplitude, velocity, and wavelength of disturbances are not necessarily independent of each other nor are they constant from one feature to the next. Given these limitations, the agreement between feature tracking and Eulerian variance is reasonable.

## REFERENCES


Anderson, D., K. I. Hodges, and B. J. Hoskins, 2003: Sensitivity of feature-based analysis methods of storm tracks to the form of background field removal. *Mon. Wea. Rev.,* **131,** 565–573.

Blackmon, M. L., 1976: Climatological spectral study of 500-mb geopotential height of Northern Hemisphere. *J. Atmos. Sci.,* **33,** 1607–1623.

——, J. M. Wallace, N. C. Lau, and S. L. Mullen, 1977: Observational study of Northern Hemisphere wintertime circulation. *J. Atmos. Sci.,* **34,** 1040–1053.

Chang, E. K. M., 2001: GCM and observational diagnoses of the seasonal and interannual variations of the Pacific storm track during the cool season. *J. Atmos. Sci.,* **58,** 1784–1800.

——, 2005: The impact of wave packets propagating across Asia on Pacific cyclone development. *Mon. Wea. Rev.,* **133,** 1998–2015.

——, and S. W. Song, 2006: The seasonal cycles in the distribution of precipitation around cyclones in the western North Pacific and Atlantic. *J. Atmos. Sci.,* **63,** 815–839.

——, and P. Zurita-Gotor, 2007: Simulating the seasonal cycle of the Northern Hemisphere storm tracks using idealized nonlinear storm-track models. *J. Atmos. Sci.,* **64,** 2309–2331.

Chen, S. J., Y. H. Kuo, P. Z. Zhang, and Q. F. Bai, 1991: Synoptic climatology of cyclogenesis over East Asia, 1958–1987. *Mon. Wea. Rev.,* **119,** 1407–1418.

Christoph, M., U. Ulbrich, and P. Speth, 1997: Midwinter suppression of Northern Hemisphere storm track activity in the real atmosphere and in GCM experiments. *J. Atmos. Sci.,* **54,** 1589–1599.

Deng, Y., and M. Mak, 2005: An idealized model study relevant to the dynamics of the midwinter minimum of the Pacific storm track. *J. Atmos. Sci.,* **62,** 1209–1225.

Donohoe, A., and D. S. Battisti, 2009: The amplitude asymmetry between synoptic cyclones and anticyclones: Implications for filtering methods in feature tracking. *Mon. Wea. Rev.,* **137,** 3874–3887.

Eady, E. T., 1949: Long waves and cyclone waves. *Tellus,* **1,** 33–42.

Hakim, G., 2003: Developing wave packets in the North Pacific storm track. *Mon. Wea. Rev.,* **131,** 2824–2837.

Harnik, N., and E. K. M. Chang, 2004: The effects of variations in jet width on the growth of baroclinic waves: Implications for midwinter Pacific storm track variability. *J. Atmos. Sci.,* **61,** 23–40.

Hodges, K. I., 1994: A general method for tracking analysis and its application to meteorological data. *Mon. Wea. Rev.,* **122,** 2573–2586.

——, 1995: Feature tracking on the unit sphere. *Mon. Wea. Rev.,* **123,** 3458–3465.

——, 1999: Adaptive constraints for feature tracking. *Mon. Wea. Rev.,* **127,** 1362–1373.

Hoskins, B. J., and K. I. Hodges, 2002: New perspectives on the Northern Hemisphere winter storm tracks. *J. Atmos. Sci.,* **59,** 1041–1061.

——, and ——, 2005: A new perspective on Southern Hemisphere storm tracks. *J. Climate,* **18,** 4108–4129.

Ioannou, P., and R. S. Lindzen, 1986: Baroclinic instability in the presence of barotropic jets. *J. Atmos. Sci.,* **43,** 2999–3014.

Lindzen, R. S., and B. Farrell, 1980: A simple approximate result for the maximum growth rate of baroclinic instabilities. *J. Atmos. Sci.,* **37,** 1648–1654.

Nakamura, H., 1992: Midwinter suppression of baroclinic wave activity in the Pacific. *J. Atmos. Sci.,* **49,** 1629–1642.

——, and T. Sampe, 2002: Trapping of synoptic-scale disturbances into the North-Pacific subtropical jet core in midwinter. *Geophys. Res. Lett.,* **29,** 1761, doi:10.1029/2002GL015535.

——, and A. Shimpo, 2004: Seasonal variations in the Southern Hemisphere storm tracks and jet streams as revealed in a reanalysis dataset. *J. Climate,* **17,** 1828–1844.

——, T. Izumi, and T. Sampe, 2002: Interannual and decadal modulations recently observed in the Pacific storm track activity and East Asian winter monsoon. *J. Climate,* **15,** 1855–1874.

Newton, C. W., 2004: Associations between twice-yearly oscillations of the North Pacific cyclone track and upper-tropospheric circulations over the Eastern Hemisphere. *Mon. Wea. Rev.,* **132,** 348–367.

Orlanski, I., 2005: A new look at the Pacific storm track variability: Sensitivity to tropical SSTs and to upstream seeding. *J. Atmos. Sci.,* **62,** 1367–1390.

Robinson, D. P., and R. X. Black, 2006: Baroclinic development in observations and NASA GSFC general circulation models. *Mon. Wea. Rev.,* **134,** 1161–1173.

——, ——, and B. A. McDaniel, 2006: A siberian precursor to midwinter intraseasonal variability in the North Pacific storm track. *Geophys. Res. Lett.,* **33,** L15811, doi:10.1029/2006GL026458.

Roe, G., 2009: On the interpretation of Chinese loess as a paleoclimate indicator. *Quat. Res.,* **71,** 150–161.

Uppala, S. M., and Coauthors, 2005: The ERA-40 Re-Analysis. *Quart. J. Roy. Meteor. Soc.,* **131,** 2961–3012.

Wallace, J. M., G. H. Lim, and M. L. Blackmon, 1988: Relationship between cyclone tracks, anticyclone tracks, and baroclinic waveguides. *J. Atmos. Sci.,* **45,** 439–462.

Yin, J., 2002: The peculiar behavior of baroclinic waves during the midwinter suppression of the Pacific storm track. Ph.D. thesis, University of Washington, 137 pp.

Zhang, Y. Q., and I. M. Held, 1999: A linear stochastic model of a GCM's midlatitude storm tracks. *J. Atmos. Sci.,* **56,** 3416–3435.

Zurita-Gotor, P., and E. K. M. Chang, 2005: The impact of zonal propagation and seeding on the eddy–mean flow equilibrium of a zonally varying two-layer model. *J. Atmos. Sci.,* **62,** 2261–2273.